ACS APPLIED MATERIALS & INTERFACES

Research Article

www.acsami.org

Tailoring the Affinity of Organosilica Membranes by Introducing Polarizable Ethenylene Bridges and Aqueous Ozone Modification

Rong Xu,[†] Masakoto Kanezashi,[†] Tomohisa Yoshioka,[†] Tetsuji Okuda,[†] Joji Ohshita,[‡] and Toshinori Tsuru*,[†]

[†]Department of Chemical Engineering, and [‡]Department of Applied Chemistry, Hiroshima University, Higashi-Hiroshima 739-8527, Japan

Supporting Information

ABSTRACT: Bis(triethoxysilyl)ethylene (BTESEthy) was used as a novel precursor to develop a microporous organosilica membrane via the sol–gel technique. Water sorption measurements confirmed that ethenylene-bridged BTESEthy networks had a higher affinity for water than that of ethane-bridged organosilica materials. High permeance of CO_2 with high CO_2/N_2 selectivity was explained relative to the strong CO_2 adsorption on the network with π-bond electrons. The introduction of polarizable and rigid ethenylene bridges in the network structure led to improved water permeability and high NaCl rejection (>98.5%) in reverse osmosis (RO). Moreover, the aqueous ozone modification promoted significant improvement in the water permeability of the membrane. After 60 min of ozone exposure, the water permeability reached 1.1×10^{-12} $m^3/(m^2\ s\ Pa)$, which is close to that of a commercial seawater RO membrane. Meanwhile, molecular weight cutoff measurements indicated a gradual increase in the effective pore size with ozone modification, which may present new options for fine-tuning of membrane pore sizes.

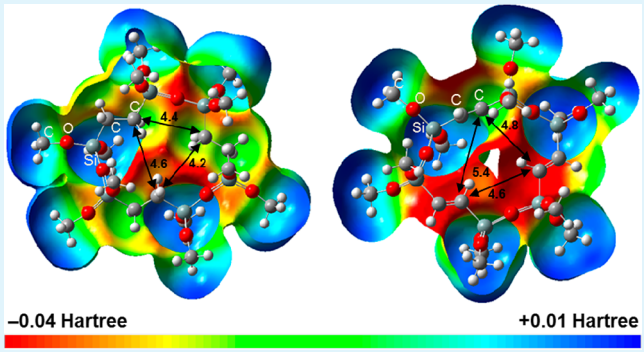

KEYWORDS: *organosilica, sol–gel, affinity, membrane, reverse osmosis, microporous*

INTRODUCTION

Because of global water scarcity and a growing demand for freshwater, the development of new and more efficient membranes for water purification is becoming an especially important task.[1,2] Polyamide-based thin film composite membranes dominate the current reverse osmosis (RO) and nanofiltration membrane markets, mainly because of their high salt rejection and high water permeability.[3] The main drawback of polyamide membranes is their susceptibility against chlorine, which is the most widely used disinfectant or as a membrane cleaning agent.[4] Therefore, numerous attempts have been made to explore robust RO membranes with high permeability and selectivity, as well as improved durability. Zeolite membranes (silicalite and ZSM-5) with good chemical resistance have successfully been explored for RO removal of salt ions and small organic molecules from water. In general, superior rejection has been achieved via charge- and/or size-based exclusion, but these zeolite membranes require tedious synthesis procedures to form defect-free ultrathin layers.[5−7] Microporous inorganic silica membranes are another promising candidate owing to their excellent molecular sieving ability. Highly permselective silica membranes are used in gas separation and pervaporation processes.[8,9] However, a low hydrothermal stability severely limits their application to water purification.

A significant breakthrough in hydrothermal stability came with the development of organosilica membranes, which were prepared via the hydrolysis and condensation of organically bridged bis-silyl precursors.[10−15] The introduction of covalently bridging groups into silica networks greatly improved membrane durability in water-containing system. Castricum et al.[10,11] reported a quite stable performance of 2 years for the pervaporative dehydration of butanol at 150 °C, using organosilica membranes derived from the co-condensation of bis(triethoxysilyl)ethane (BTESE) and methyltriethoxysilane. More importantly, the versatility of organic bridges offers the ability to fine-tune the chemical-physical properties of a membrane at the molecular level. We proposed a "spacer" technique to control the silica networks, where the ethane groups were introduced to design a loose structure for development of a highly permeable hydrogen separation membrane.[13] Furthermore, the influences of size, flexibility, and shape of various alkyl and aryl bridges on the membrane pore size, nanostructure, and affinity was described to determine the relationship between the bridging group and the membrane properties.[14]

Received: March 25, 2013
Accepted: June 12, 2013
Published: June 12, 2013

Recently, we examined the possibility of applying organosilica membranes to water desalination under aggressive environments. The BTESE-derived organosilica membranes exhibited exceptional hydrothermal stability at 90 °C and excellent tolerance to chlorine, showing great promise as robust RO membranes.[15] The only weakness of the BTESE membrane was the relatively low water permeability, mainly due to the hydrophobic nature of the ethane bridges, which would not allow water to rapidly pass through the membrane. Consequently, the chemical structure of the organosilica network must be altered to improve water affinity, in order to achieve a high water permeation rate. A modification strategy was only recently reported by incorporating hydrophilic amino-functionalized precursors in a BTESE matrix, which led to highly water-permeable membranes for pervaporation.[16] Yet, the co-condensation of organosilanes with terminal amine groups would result in a less durable structure and a wider pore size distribution.[17]

Here, we present the first results of development of ethenylene-bridged organosilica membranes that have improved water permeability while maintaining a high selectivity and robustness in water purification. The organosilica membranes with ethenylene (−CH═CH−) bridges were prepared from bis(triethoxysilyl)ethylene (BTESEthy), a novel precursor for membrane materials. The π-bond electrons are more polarizable in the −CH═CH− bridges than electrons of σ-bond in the alkyl bridges, making the membrane more attractive to polar water molecules. The covalently bridged network architecture also suggests superior hydrothermal stability. Moreover, the unsaturated ethenylene bridges are reactive and therefore provide plenty of opportunities for further chemical modification, such as bromination, sulfonation, and epoxidation.[18−20] In the present study, we tried a new and convenient method, that is ozone-assisted affinity modification, to further improve the water permeability of the membrane. The use of ozone treatment on periodic mesoporous organosilicas (PMOs) was recently reported by Polarz et al. for the creation of advanced, functionalized pore walls.[21] However, gas-phase ozone treatment resulted in a complete removal of the organic moieties in the ethenylene-bridged PMOs. In the present work, low levels of aqueous ozone were utilized to modify the innovative BTESEthy membranes.

EXPERIMENTAL SECTION

Sol Synthesis. 1,2-Bis(triethoxysilyl)ethylene (BTESEthy, 95%, ~80% trans isomer, Gelest, Inc.) sol was synthesized by hydrolysis and polymerization reaction of a precursor $(EtO)_3SiCH{=}CHSi(OEt)_3$ with water and HCl, in ethanol. A required amount of BTESEthy was mixed with ethanol. Subsequently, premixed water and HCl were added dropwise to the precursor mixture under continuous stirring. The molar composition of the reactants was BTESEthy/H_2O/HCl = 1:60:0.1, and the weight percent of BTESEthy was kept at 5.0 wt %. The solution was stirred for 2 h at 25 °C before coating. BTESEthy-derived gel powder was prepared by drying at 40 °C in air, and was ground using a mortar. 1,2-Bis(triethoxysilyl)ethane (BTESE) sol and gel powder were prepared under the same conditions as the BTESEthy.

Membrane Preparation. Tubular α-alumina microfiltration membranes (Mitsui Grinding Wheel Company; porosity, 50%; average pore size, 1 μm; outside diameter, 10 mm; and length, 100 mm) were used as the supports. The detailed procedure for synthesis of SiO_2−ZrO_2 colloidal sols was described elsewhere.[22] First, two kinds of α-alumina particles (average particle sizes were 1.9 and 0.2 μm, respectively) were deposited onto the outer surface of the support using the SiO_2−ZrO_2 colloidal sol (2 wt.%) as a binder, and the substrate was fired at 550 °C for 30 min. This procedure was repeated 6 times to form the particle layer. Then, SiO_2−ZrO_2 (molar ratio of Si/Zr = 1/1, 0.5 wt %) colloidal sols were coated onto the particle layer via a hot-coating method,[22] where the substrate was first heated up to around 180 °C before coating, followed by quickly contacting the substrate with a wet cloth with the SiO_2−ZrO_2 sols. Subsequently, the substrate was fired at 550 °C for 15 min in air. This hot-coating and calcination procedures were repeated approximately 6 times to form the intermediate layer. Finally, the BTESEthy sol (0.5 wt %) was coated onto the intermediate layer in a manner similar to the SiO_2−ZrO_2 sol, followed by flash calcination at 300 °C in air for 20 min.

Characterization. The size distribution of the sols was measured by dynamic light scattering (DLS) at 25 °C using a Malvern Zetasizer Nano-ZS (ZEN3600). Thermogravimetric/differential thermal analysis (TG/DTA) was carried out in air using a DTG-60 instrument with a heating rate of 10 °C min^{-1}. The membrane structure and morphology were examined by field-emission scanning electron microscopy (FE-SEM, S-4800) with an acceleration voltage of 15 kV. X-ray photoelectron spectroscopy (XPS, ESCA3400) measurements were performed on the membrane sample that was used for SEM analysis. Depth profiles of the concentrations of C, Si, and Zr in the membrane were calculated from the C 1s, Si 2p and Zr 3d energy bands via sputtering with 0.6 kV Ar^+ at 80 nm min^{-1}. Fourier Transform Infrared Spectrometer (FT/IR-4100) was applied to confirm the chemical structure of the BTESEthy films before and after ozone exposure. Films for FTIR and static contact angle (CA) measurements were obtained by coating the organosilica sols onto clean silicon wafers, followed by calcination at 300 °C for 20 min. The microstructures and surface properties of the organosilica networks were studied by nitrogen (at 77 K) and water sorption (at 298 K), respectively, using a Belsorp-Max (Bel Japan, Inc.) instrument. Before analysis, the samples were outgassed at 200 °C overnight under vacuum. The Brunauer−Emmett−Teller (BET) method in the relative pressure range of P/P_0 = 0.01−0.25 was used to calculate the specific surface area. The pore size distribution was obtained through the analysis of the adsorption branch of nitrogen isotherms using the MP method. The micropore volume was estimated using the *t*-plot method.

Membrane Performance. Single gas permeation measurements were performed at 200, 150, 100, and 50 °C in this sequence, using high-purity of He, H_2, CO_2, N_2, C_3H_6, C_3H_8, and SF_6. Prior to measurement, the membrane was dried for 8 h at 200 °C in a He flow of 20 mL min^{-1}. The permeate stream was kept at atmospheric pressure, and the pressure drop through the membrane was maintained at 1 bar. The permeation rate was measured using a soap-film flow meter.

Water desalination experiments were carried out using a 2,000 ppm NaCl solution, and molecular weight cutoff (MWCO) measurements were performed using 500 ppm neutral solutes: ethanol, isopropanol, glucose, and sucrose. RO experiments were conducted at 25 °C, unless otherwise specified, using a typical RO testing apparatus as previously described.[23] The feed solution, pressurized with a plunger pump, was vigorously agitated in the RO cell, and the retentate was recycled at an approximate flow of 30 mL min^{-1}. Water permeability, L_p, was calculated from the volume flux, J_v, divided by the effective transmembrane pressure, $\Delta P-\Delta\pi$, as follows.

$$J_v = L_p(\Delta P - \Delta\pi)$$

where L_p is the water permeability and, ΔP ($=P_1 - P_2$) and $\Delta\pi$ ($=\pi_1 - \pi_2$) are the differences in applied pressure and osmotic pressure, respectively. The observed rejection, R_{obs}, can be expressed as follows

$$R_{obs} = (1 - C_p/C_f) \times 100\%$$

The concentrations of feed (C_f) and permeate (C_p) were measured with a conductivity meter for NaCl and a total organic carbon analyzer (Shimadzu, TOC-V_E) for neutral solutes. Each RO test was first run for at least 3 h to confirm a steady state, and the membrane performance was then measured. Each experimental data point presented in this study is the average value of 3 samples. The

deviation in data of water permeability and observed rejection was found to be less than 4.2 and 0.6%, respectively.

Ozone Modification. The ozone treatment experiments were performed using the setup shown in Figure S1 (see the Supporting Information). Ozone was produced from high-purity oxygen gas using an ozone generator (Fuji Electric, PO-10), which allowed control of the ozone concentration and the flow rate. Ozone must be injected continuously into the water due to its instability. A preinjection of about 3 h was required to establish a steady level of dissolved ozone. The concentration of ozone in water was maintained at 1 ppm, which was periodically analyzed using the indigo method.[24] BTESEthy membranes were periodically soaked in the aqueous ozone system for a predetermined time interval. The filtration performances were then evaluated after rinsing with deionized water.

RESULTS AND DISCUSSION

Size distribution of the BTESEthy sol with a silica concentration of 0.3 mol L^{-1} was determined by dynamic light scattering at 25 °C, as presented in Figure 1. The freshly

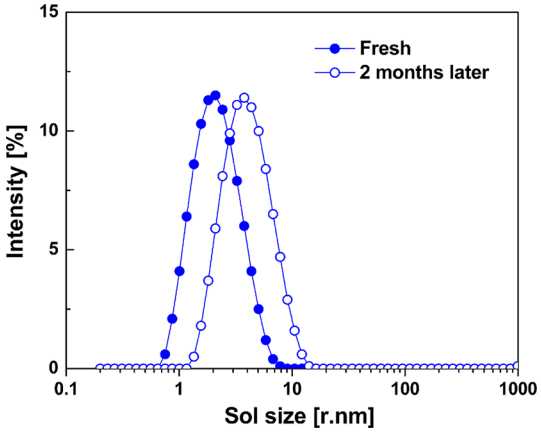

Figure 1. Size distribution of the BTESEthy sol determined by DLS.

synthesized BTESEthy sol showed a small mean radius of 2.1 nm and a narrow monomodal size distribution, which was desirable for preparing a thin, microporous separation layer. After storage at 0 °C for 2 months, only a slight increase in mean particle size was observed, ranging from 2.1 to 3.7 nm, with no broadening of the size distribution. The slight increase in size was probably dominated by the polymerization reaction of the monomer species, rather than by the aggregation of nanoparticals, because even a very small fraction of aggregation would result in a dramatic size increase in the sol and a broadening of its size distribution.[14,25]

TG/DTA was conducted to evaluate the thermal stability of the ethenylene-bridged network in air (see Figure S2 in the Supporting Information). The TG curve shows that a weight loss occurred in three steps. The first weight loss of about 14% below ~150 °C was assigned to the removal of physisorbed water. A minor weight loss of ~5% was observed for temperatures ranging from 150 to 350 °C, most likely due to an ongoing condensation reaction of the silanol groups (dehydroxylation)[26] and the desorption of small amounts of chemisorbed water. Above approximately 350 °C, a continuous decrease in weight (~10%) was attributed to the decomposition of organic groups in the network (as revealed by the exothermic DTA peak). The BTESEthy material was confirmed to be thermally stable up to ~350 °C in air atmosphere.

To probe the pore structure, the N_2 adsorption−desorption isotherms of BTESEthy together with BTESE for a comparison, are presented in Figure 2a. Both of the N_2 isotherms show type-I characteristics, with a significant uptake of N_2 at low relative pressure, which is typical of microporous materials. No hysteresis was observed in the isotherms, indicating the absence of mesopores.[27] Details of the physicochemical properties are given in Table 1. The BTESEthy sample exhibited a higher BET specific surface area together with a slightly larger volume of micropores, compared with the BTESE material. The incorporation of ethenylene bridges imparted higher rigidity within the networks, which prevented the collapse of pores and the formation of dead-end pores during the calcination process, hence affording a more open and accessible pore structure.[28,29] Both materials had a narrow pore size distribution with a maximum at the nominal pore diameter of 0.6 nm (Figure 2b), which is in good agreement with an effective pore size of ~0.5 nm as estimated by gas permselectivities for the BTESE membrane.[30]

Figure 2c shows the water sorption isotherms of BTESE and BTESEthy materials measured at 298 K. Overall, a higher sorption capacity of water (366 cm^3 g^{-1}) was observed for BTESEthy, partly because of its larger surface area. In addition, the nonclosed isotherms demonstrated that the adsorbed water could not completely desorb from the pore surface of the network, suggesting a strong chemisorption of water molecules in the two materials. Because the chemisorption at low pressure is primarily driven by water vapor loading, whereas physisorption at high pressure depends mainly on the surface area, the differences in sorption behavior at low pressure are more significant for a confirmation of the internal water affinity of the two kinds of networks. Thus, the water sorption capacities normalized by their specific surface area were further compared at a low water vapor pressure of up to 0.1 atm (Figure 2d). Apparently, a more rapid growth of water uptake was observed for BTESEthy, demonstrating a stronger water affinity of the internal network. The results were consistent with the contact angles of the thin films (Table 1), which also showed a higher surface hydrophilicity of the BTESEthy material.

Figure 3 shows a cross-sectional SEM image of a BTESEthy-derived organosilica membrane. Although it is difficult to distinguish the uppermost separation layer from the SiO_2−ZrO_2 intermediate layer, a thin and defect-free separation layer can be observed on top of the intermediate layer, with a total thickness of approximately 200 nm. The thickness of the BTESEthy-derived separation layer was further confirmed by the XPS depth profile analysis (Figure 4). The concentration of C atoms that is attributed to Si−CH═CH−Si bonds was detected on the membrane surface and showed a sharp decrease at a depth from 0 to 60 nm. This suggested that the effective separation layer had a thickness of about 60 nm. The concentration of Zr, which was obtained from the SiO_2−ZrO_2 intermediate layer, was also detected near the surface and increased with an increase in depth. Considering the small size of BTESEthy sol, the penetration of the organosilica sol would occur during the coating procedure, resulting in an atomic mixing of C and Zr in the top layer of the membrane.

To investigate the separation efficiency of the BTESEthy membrane, the temperature dependence of gas permeances was measured using He, H_2, CO_2, N_2, C_3H_6, C_3H_8, and SF_6 in different molecular sizes (see Figure S3 in the Supporting Information). On the whole, the permeances of He, H_2, and N_2 decreased as temperature decreased, which is typical for activated permeation. In contrast, for adsorptive molecules

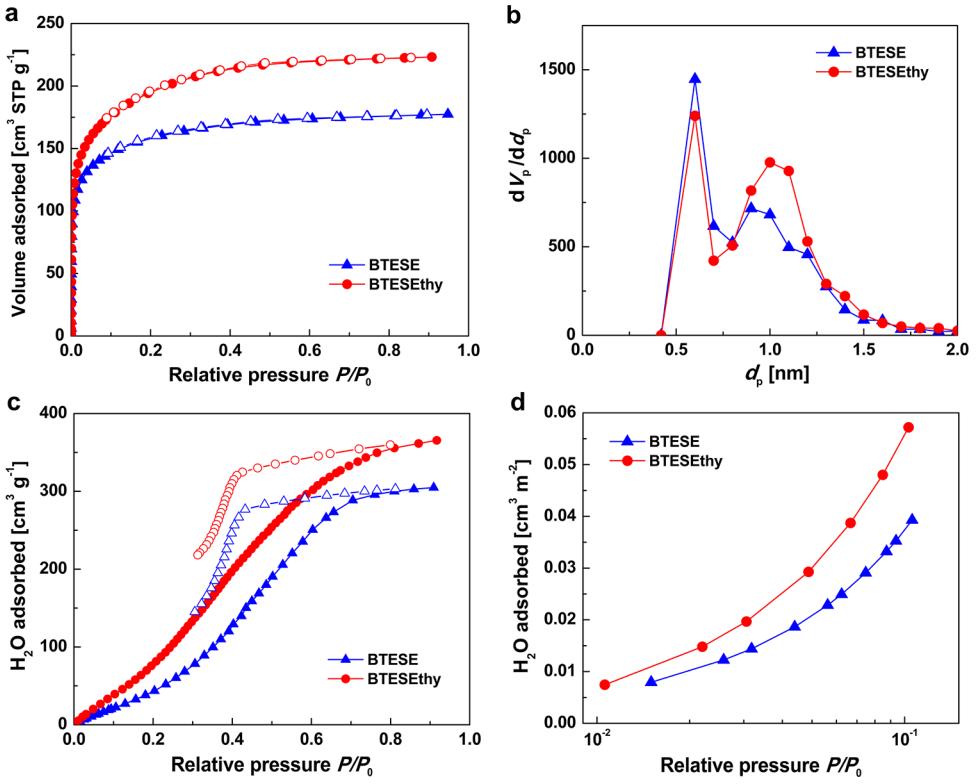

Figure 2. (a) Nitrogen adsorption−desorption isotherms of BTESE and BTESEthy samples (77 K) and (b) pore size distribution (calculated by MP method). (c) Water sorption isotherms of the samples (298 K) and (d) plots of samples at low pressure normalized to their specific surface area.

Table 1. Physicochemical Properties of BTESE and BTESEthy Materials

sample	BET surface area A_{BET} (m^2/g)	micropore volume V_p (cm^3/g)	micropore diameter d_p (nm)	contact angles of films CA (deg)
BTESE	571	0.27	0.6	66.8 ± 1.4
BTESEthy	696	0.34	0.6	50.4 ± 2.1

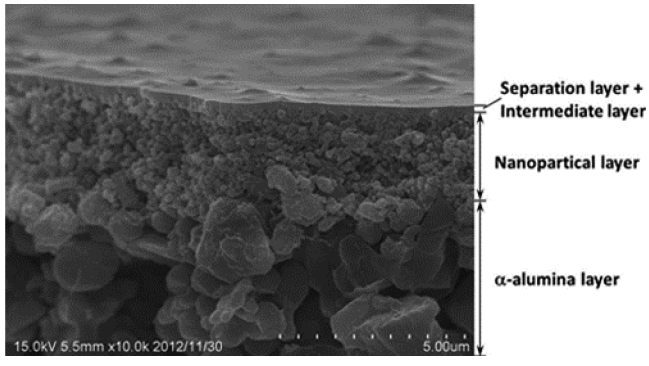

Figure 3. Cross-sectional SEM image of a BTESEthy membrane.

such as CO_2, C_3H_6, C_3H_8, and SF_6, the permeances generally increased with decreasing temperature. This tendency may be caused by the adsorption effects, as the concentration gradient by adsorption increased with decreasing temperature. It is worth noting that the permeances of CO_2 and C_3H_6 appeared to peak at 100 °C, which can be explained by the balance between adsorption and diffusivity as follows. The number of adsorbed molecules increased as temperature decreased. Conversely, the enhanced adsorption caused a decrease in mobility at temperatures lower than the peak, hindering the

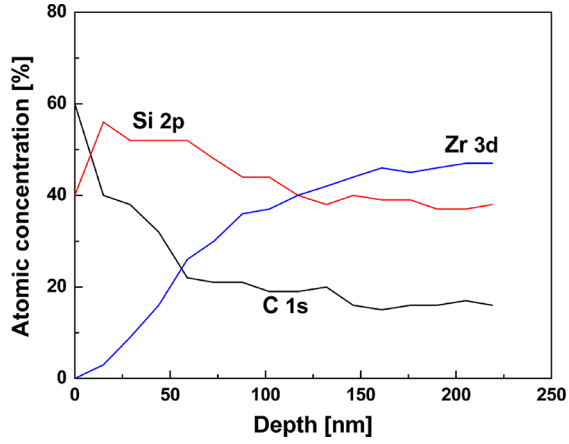

Figure 4. Depth profile of C 1s, Si 2p, and Zr 3d in the BTESEthy membrane.

diffusion of molecules through the membrane (liquidlike diffusion of pore filling molecules).[31]

We further calculated the relevant permeance ratios of H_2/N_2, CO_2/N_2, and C_3H_6/C_3H_8 at various temperatures, as listed in Table 2. The BTESEthy membrane exhibited the highest H_2/N_2 permeance ratio of 39.5 at 200 °C, indicating the

Table 2. Gas Permeance Ratios through the BTESEthy Membrane at Different Temperatures

selectivity	50 °C	100 °C	200 °C
H_2/N_2	21.1	38.7	39.5
CO_2/N_2	32.7	23.3	9.6
C_3H_6/C_3H_8	2.7	4.4	4.4

dx.doi.org/10.1021/am401056a | ACS Appl. Mater. Interfaces 2013, 5, 6147−6154

superior molecular sieving ability of the network structure. Surprisingly, a high permeance of CO_2 was observed (See Figure S3 in the Supporting Information), with the highest CO_2/N_2 selectivity of 32.7 at 50 °C, which was due to the strong adsorption of CO_2 on the network with π-bond electrons. Therefore, the BTESEthy membrane showed great potential for CO_2 separation. Additionally, the $\pi-\pi$ interaction between the ethenylene bridges and the C_3H_6 molecules may contribute to a preferential C_3H_6 adsorption on the BTESEthy membrane, considering that the molecular sizes of C_3H_6 and C_3H_8 are quite close.

The superior sieving ability and higher water affinity of BTESEthy membranes prompted us to study their desalination performances. The RO desalination performances were evaluated using a 2000 ppm NaCl solution at a pressure that varied from 0.7 to 1.5 MPa (Figure 5). As the operating

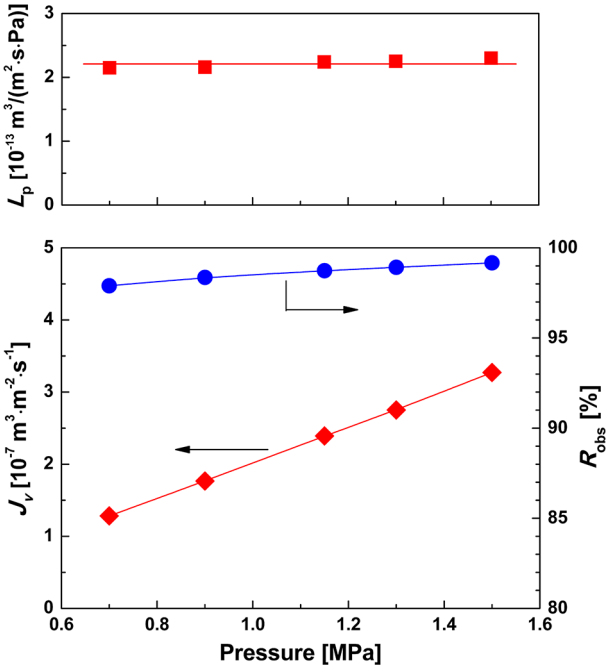

Figure 5. Effect of operating pressure on water flux, salt rejection, and water permeability.

pressure increased, the water flux (J_v) and the salt rejection (R_{obs}) of the BTESEthy membrane increased continuously, whereas the water permeability (L_p) remained almost constant at approximately 2.2×10^{-13} $m^3/(m^2\ s\ Pa)$. This can be well explained by the solution-diffusion (SD) model.[32] The transmembrane pressure difference ($\Delta P-\Delta\pi$) is the driving force for water transport across the membrane. Thus, the water flux increased linearly with an increase in the operating pressure, while water permeability, L_p, remained almost constant. However, the ion permeation, according to the SD model, was independent of the operating pressure. As the pressure increased, the enhanced water permeation led to an increase in salt rejection from 97.9 to 99.2%.

Chlorine resistance experiments were performed on the BTESEthy membrane by soaking tests (see more experimental details in the Supporting Information). The BTESEthy membrane exhibited excellent chlorine tolerance owing to the inherently stable organosilica network, which lacks chemical functionalities that are susceptible to chlorine attack (see Figure S4 in the Supporting Information). After a total chlorine exposure of as much as 21 000 ppm h, there was no obvious change in the NaCl rejection. In contrast, the rejection of the commercial polyamide RO membrane dropped dramatically after only ~7000 ppm h of chlorine exposure.[33] This high chlorine tolerance of BTESEthy membranes may offer great advantages over the commercial polyamide RO membranes. Furthermore, the temperature cycle experiment demonstrated good hydrothermal stability for the BTESEthy membrane (see Figure S5 in the Supporting Information).

To further improve the water permeability, ozone-assisted modification was examined on the BTESEthy membranes. In these experiments, the membranes were periodically exposed to a 1 ppm level of ozone aqueous solution for a certain period of time. Figure 6 illustrates the water permeability and NaCl

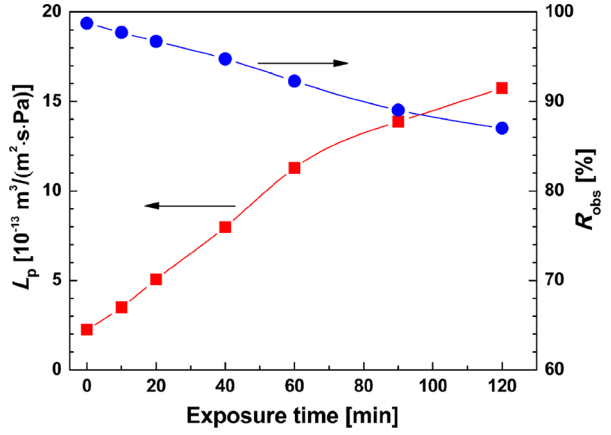

Figure 6. Effect of ozone treatment on water permeability and salt rejection at an operating pressure of 1.15 MPa.

rejection as a function of ozone exposure. The water permeability increased continuously with exposure time, and the rejection decreased gradually. After a total exposure of 2 h, the water permeability of the membrane increased more than 7-fold, and the salt rejection decreased from 98.8% to 87.1% due to the increased permeation of NaCl. The substantial improvement in water permeability can be explained by the change in chemical structures, as confirmed by FTIR analysis of the BTESEthy films (Figure 7). The following characteristic bands were mainly related to the BTESEthy framwork: C−H

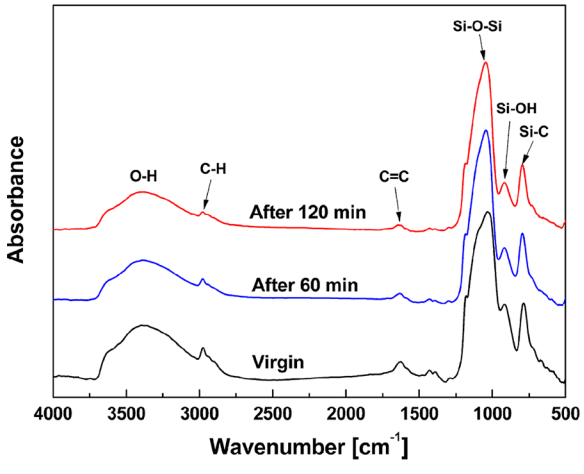

Figure 7. FTIR spectra of the BTESEthy film before and after ozone treatment.

dx.doi.org/10.1021/am401056a | ACS Appl. Mater. Interfaces 2013, 5, 6147−6154

stretching vibrations in the vinyl unit (~2980 cm^{-1}); C═C stretch (~1620 cm^{-1}); Si−O−Si stretch (1020−1200 cm^{-1}); Si−OH stretch (~920 cm^{-1}); and Si−C stretch (~790 cm^{-1}).[34,35] Obviously, a decrease in the intensities of C═C stretching vibrations was observed with exposure time (See quantitative data in Table S1 in the Supporting Information), indicative of the reaction of the C═C bond with ozone. The mechanism for the ozonolysis of ethenylene-bridged organosilicas was discussed in detail by Polarz and his co-workers.[21] Ozone treatment resulted in cleavage of the C═C and Si−C bonds and eventually in the formation of new silanol groups. The formation of silanol groups in the organosilica network greatly enhanced the H_2O-affinity of the membrane, thus leading to high water permeability. Unlike the gas-phase ozone treatment,[21] ethenylene bridges in the network did not completely react with the aqueous ozone in this study. Even after ozone exposure for 120 min, the characteristic C═C vibration bands could be observed in the FTIR spectra (Figure 7). A more likely explanation is that the ethenylene bridges exposed on the surface of channel walls seemed to preferentially react with the aqueous ozone, and the bridging groups embedded inside the channel walls remained, probably because of very low levels of ozone and limited exposure time.

With respect to molecular separation membranes, we concentrated more on the effective pore size change after ozone modification, which was reflected by molecular weight cutoff (MWCO). Figure 8 shows the change in the MWCO of

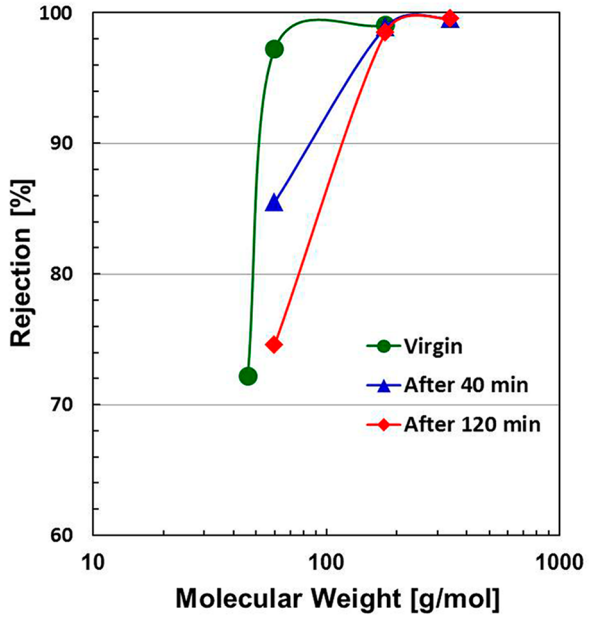

Figure 8. Change of MWCO curves after ozone treatment.

the BTESEthy membrane, using a series of neutral solutes of different sizes: ethanol (Stokes diameter (Sd): 0.4 nm), isopropanol (Sd: 0.48 nm), glucose (Sd: 0.73 nm), and sucrose (Sd: 0.94 nm).[36] The MWCO, defined at 90% rejection, of the virgin membrane was approximately 50 Da. Clearly, with an increase in the ozone treatment time, the MWCO increased to ca. 90 Da after 40 min, and further increased to ca. 120 Da after 120 min, indicating a gradual increase in effective membrane pore size. Despite a decrease in NaCl rejection due to the increased pore size, the BTESEthy membrane was still capable of molecular sieving for large molecules such as glucose and sucrose with rejection higher than 98%, showing good potential for applications such as removal of organics and nanofiltration. Therefore, ozone modification may present new options for tailoring membrane pore sizes according to specific separation requirements.

Figure 9 shows the trade-off relationship between NaCl rejection and water permeability for zeolite and organosilica

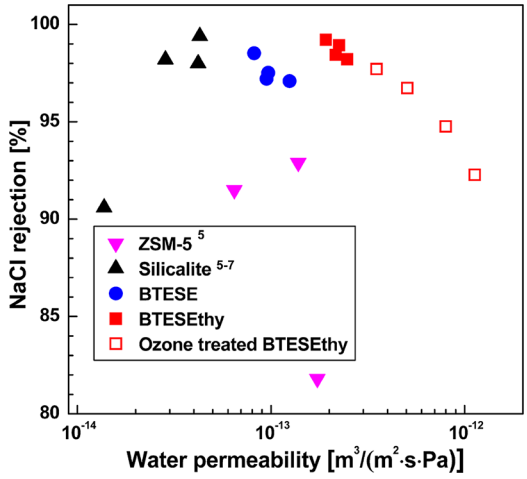

Figure 9. Trade-off of desalination performances for zeolite (25 °C, 2.76 MPa, and 0.1 M NaCl) and organosilica (25 °C, 1.15 MPa, and 2000 ppm NaCl) RO membranes.

RO membranes. Generally speaking, BTESEthy-derived organosilica membranes showed better desalination performance than typical zeolite RO membranes such as ZSM-5 and silicalite. Even at a low pressure of 1.15 MPa, BTESEthy membranes almost completely (>98.5%) rejected NaCl. Compared to BTESE membranes, the water permeability of BTESEthy membranes was approximately doubled with no drop in rejection, simply by adjusting the bridging groups of the network. To elucidate the electron density distribution and the structure of the BTESE and BTESEthy networks, quantum chemical calculations were carried out (see details in the Supporting Information). For the calculations, model molecules with a trimeric 15-membered ring structure (see Figure S6 in the Supporting Information) were employed because these seem to be the smallest strain-free systems among the cyclic oligomers. The siloxy linkages on the silicon atoms in the real systems were replaced by methoxy groups in the models for simplification to minimize the computation time. The optimized geometries have a rather round-shaped cyclic structure, but for the BTESEthy model, the ring is slightly ellipsoidal (Figure 10). The shortest inner ring through space C···C distance was 4.6 Å for the BTESEthy model, whereas that for the BTESE model was 4.2 Å, suggesting a more open pore structure of the BTESEthy system, probably because of the increased rigidity in the ethenylene-bridged network. The electrostatic potentials (ESPs) of both models showed that the negative potentials were mainly localized inside the rings. However, the BTESEthy model exhibited a higher contrast for positive and negative potentials, compared with the BTESE model, which led to an enhanced H_2O-affinity for the BTESEthy channels by hydrogen-bonding and/or dipole−dipole interaction. Furthermore, as presented in Figure 9, the water permeability of the BTESEthy membranes was significantly improved by a simple ozone modification. For

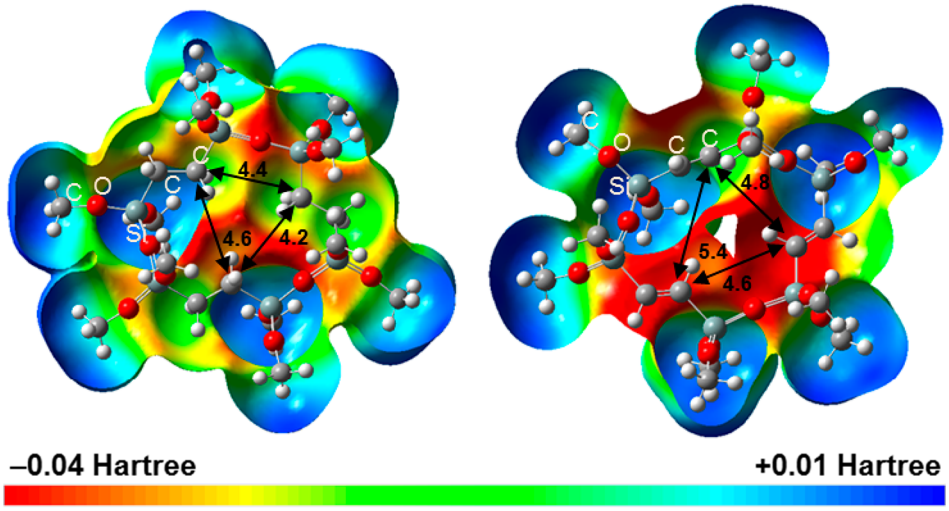

Figure 10. Optimized structures and ESPs for models of (left) BTESE and (right) BTESEthy networks. Numbers indicate through space inner ring C···C distances/Å. Colors range from −0.04 to +0.01 hartree with orange and blue denoting extremely electron-rich and -deficient regions, respectively.

example, despite a moderate rejection decrease from 98.8 to 92.3% after a 60 min exposure, the water permeability reached 1.1×10^{-12} $m^3/(m^2\ s\ Pa)$, close to that of the commercial seawater RO membrane SW30HR.[37] Further studies are focused on other chemical modifications on the versatile BTESEthy membranes to simultaneously improve water permeability and salt rejection.

CONCLUSIONS

An ethenylene-bridged microporous organosilica membrane has been developed and applied in reverse osmosis (RO). A thin and defect-free separation layer was obtained by optimizing the sol synthesis. Because of the introduction of ethenylene bridges in the network, the BTESEthy material exhibited a large BET surface area and superior water affinity. In gas permeation measurements, a high permeance of CO_2 with high CO_2/N_2 selectivity was observed for BTESEthy membranes at low temperatures, which shows great promise for CO_2 separation applications. RO tests demonstrated that increasing the operating pressure resulted in a continuous increase in flux and salt rejection, whereas water permeability remained almost constant. BTESEthy membranes exhibited excellent chlorine resistance because of the stable organically bridged network structure. Moreover, a significant improvement in water permeability was achieved by the aqueous ozone modification of the BTESEthy membrane, due to the great enhancement of water affinity by the reaction of the ethenylene bridges with ozone. Meanwhile, the effective pore size increased gradually with the ozone modification, which could present new options for tailoring membrane pore sizes. Compared with BTESE membranes, when using BTESEthy membranes, a simple adjustment of the linkages to the more polarizable and rigid ethenylene bridges doubled the water permeability with no drop in rejection.

ASSOCIATED CONTENT

Supporting Information

Experimental setup for ozone modification, thermal stability, gas permeation properties, chlorine resistance and hydrothermal stability of the BTESEthy membranes, the change in absorbance values, and model molecules for quantum chemical calculations. This material is available free of charge via the Internet at http://pubs.acs.org.

AUTHOR INFORMATION

Corresponding Author

*E-mail: tsuru@hiroshima-u.ac.jp.

Notes

The authors declare no competing financial interest.

ACKNOWLEDGMENTS

This research is supported in part by Core Research for Evolutional Science and Technology (CREST) Program of Japan Science and Technology Agency (JST).

REFERENCES

(1) Elimelech, M.; Phillip, W. A. *Science* **2011**, *333*, 712−717.
(2) Shannon, M. A.; Bohn, P. W.; Elimelech, M.; Georgiadis, J. G.; Marinas, B. J.; Mayes, A. M. *Nature* **2008**, *452*, 301−310.
(3) Li, D.; Wang, H. T. *J. Mater. Chem.* **2010**, *20*, 4551−4566.
(4) Glater, J.; Hong, S. K.; Elimelech, M. *Desalination* **1994**, *95*, 325−345.
(5) Li, L. X.; Liu, N.; McPherson, B.; Lee, R. *Ind. Eng. Chem. Res.* **2007**, *46*, 1584−1589.
(6) Li, L. X.; Dong, J. H.; Nenoff, T. M. *Sep. Purif. Technol.* **2007**, *53*, 42−48.
(7) Liu, N.; Li, L. X.; McPherson, B.; Lee, R. *J. Membr. Sci.* **2008**, *325*, 357−361.
(8) de Vos, R. M.; Verweij, H. *Science* **1998**, *279*, 1710−1711.
(9) Nair, B. N.; Keizer, K.; Suematsu, H.; Suma, Y.; Kaneko, N.; Ono, S.; Okubo, T.; Nakao, S. I. *Langmuir* **2000**, *16*, 4558−4562.
(10) Castricum, H. L.; Sah, A.; Kreiter, R.; Blank, D. H. A.; Vente, J. F.; ten Elshof, J. E. *Chem. Commun.* **2008**, 1103−1105.
(11) Castricum, H. L.; Sah, A.; Kreiter, R.; Blank, D. H. A.; Vente, J. F.; ten Elshof, J. E. *J. Mater. Chem.* **2008**, *18*, 2150−2158.
(12) Kreiter, R.; Rietkerk, M. D. A.; Castricum, H. L.; van Veen, H. M.; ten Elshof, J. E.; Vente, J. F. *ChemSusChem* **2009**, *2*, 158−160.
(13) Kanezashi, M.; Yada, K.; Yoshioka, T.; Tsuru, T. *J. Am. Chem. Soc.* **2009**, *131*, 414−415.
(14) Castricum, H. L.; Paradis, G. G.; Mittelmeijer-Hazeleger, M. C.; Kreiter, R.; Vente, J. F.; ten Elshof, J. E. *Adv. Func. Mater.* **2011**, *21*, 2319−2329.
(15) Xu, R.; Wang, J. H.; Kanezashi, M.; Yoshioka, T.; Tsuru, T. *Langmuir* **2011**, *27*, 13996−13999.

(16) Paradis, G. G.; Kreiter, R.; van Tuel, M. M. A.; Nijmeijer, A.; Vente, J. F. *J. Mater. Chem.* **2012**, *22*, 7258−7264.
(17) Barczak, M.; Borowski, P.; Dąbrowski, A. *Colloids Surf., A* **2009**, *347*, 114−120.
(18) Melde, B. J.; Holland, B. T.; Blanford, C. F.; Stein, A. *Chem. Mater.* **1999**, *11*, 3302−3308.
(19) Nakajima, K.; Tomita, I.; Hara, M.; Hayashi, S.; Domen, K.; Kondo, J. N. *Adv. Mater.* **2005**, *17*, 1839−1842.
(20) Sasidharan, M.; Bhaumik, A. *ACS Appl. Mater. Interfaces* **2013**, *5*, 2618−2625.
(21) Polarz, S.; Jeremias, F.; Haunz, U. *Adv. Funct. Mater.* **2011**, *21*, 2953−2959.
(22) Asaeda, M.; Yang, J. H.; Sakou, Y. *J. Chem. Eng. Jpn.* **2002**, *35*, 365−371.
(23) Xu, R.; Wang, J. H.; Kanezashi, M.; Yoshioka, T.; Tsuru, T. *AIChE J.* **2013**, *59*, 1298−1307.
(24) Bader, H.; Hoigne, J. *Water Res.* **1981**, *15*, 449−456.
(25) Tobler, D. J.; Shaw, S.; Benning, L. G. *Geochim. Cosmochim. Acta* **2009**, *73*, 5377−5393.
(26) Zhuravlev, L. T. *Colloids Surf., A* **2000**, *173*, 1−38.
(27) Jaroniec, M.; Kruk, M.; Olivier, J. P. *Langmuir* **1999**, *15*, 5410−5413.
(28) Loy, D. A.; Carpenter, J. P.; Yamanaka, S. A.; McClain, M. D.; Greaves, J.; Hobson, S.; Shea, K. J. *Chem. Mater.* **1998**, *10*, 4129−4140.
(29) Shea, K. J.; Loy, D. A. *Chem. Mater.* **2001**, *13*, 3306−3319.
(30) Kanezashi, M.; Yada, K.; Yoshioka, T.; Tsuru, T. *J. Membr. Sci.* **2010**, *348*, 310−318.
(31) Takata, Y.; Tsuru, T.; Yoshioka, T.; Asaeda, M. *Microporous Mesoporous Mater.* **2002**, *54*, 257−268.
(32) Wijmans, J. G.; Baker, R. W. *J. Membr. Sci.* **1995**, *107*, 1−21.
(33) Park, H. B.; Freeman, B. D.; Zhang, Z. B.; Sankir, M.; McGrath, J. E. *Angew. Chem., Int. Ed.* **2008**, *47*, 6019−6024.
(34) Esquivel, D.; De Canck, E.; Jimenez-Sanchidrian, C.; Van Der Voort, P.; Romero-Salguero, F. J. *J. Mater. Chem.* **2011**, *21*, 10990−10998.
(35) Sankaraiah, S.; Lee, J. M.; Kim, J. H.; Choi, S. W. *Macromolecules* **2008**, *41*, 6195−6204.
(36) Wang, X. L.; Tsuru, T.; Nakao, S.; Kimura, S. *J. Membr. Sci.* **1997**, *135*, 19−32.
(37) Hatakeyama, E. S.; Gabriel, C. J.; Wiesenauer, B. R.; Lohr, J. L.; Zhou, M. J.; Noble, R. D.; Gin, D. L. *J. Membr. Sci.* **2011**, *366*, 62−72.